Low-energy elastic electron interactions with pyrimidine

Prasanga Palihawadana, James Sullivan, Michael Brunger, Carl Winstead, Vincent McKoy, Gustavo Garcia, F. Blanco, and Stephen Buckman

Phys. Rev. A **84**, 062702 — Published 2 December 2011

DOI: 10.1103/PhysRevA.84.062702

Low Energy Elastic Electron Interactions with Pyrimidine

Prasanga Palihawadana[1], James Sullivan[1], Michael Brunger[2,3], Carl Winstead[4], Vincent McKoy[4], Gustavo Garcia[5], F. Blanco[6] and Stephen Buckman[1]

[1]Centre for Antimatter-Matter Studies, Research School of Physics and Engineering, The Australian National University, Canberra, ACT 0200, Australia

[2]Centre for Antimatter-Matter Studies, Flinders University, GPO Box 2100, Adelaide, South Australia 5001

[3]Institute of Mathematical Sciences, University of Malaya, 50603, Kuala Lumpur, Malaysia

[4]A A Noyes Laboratory of Chemical Physics, California Institute of Technology, Pasadena, CA 91125, USA

[5]Consejo Superior de Investigaciones Científicas, Serrano 113-bis, 28006 Madrid, Spain

[6]Departamento de Fisica Atomica, Molecular y Nuclear, Universidad Complutense de Madrid, 28040 Madrid, Spain

ABSTRACT: We present results of measurements and calculations of elastic electron scattering from pyrimidine in the energy range 3-50 eV. Absolute differential and integral elastic cross sections have been measured using a crossed electron-molecule beam spectrometer and the relative flow technique. The measured cross sections are compared with results of calculations using the well-known Schwinger variational technique and an independent-atom model. Agreement between the measured differential cross sections and the results of the Schwinger calculations is good at lower energies but less satisfactory at higher energies where inelastic channels that should be open are kept closed in the calculations.

1. Introduction

The importance of the role played by low-energy electrons in radiation damage on biological systems has been the subject of both experimental and theoretical investigations in the last decade [1]. This has been driven by the recognition that electrons at sub-ionization [2] or even sub-excitation energies [3] have the ability to break DNA strands. Because secondary electrons with energies below 20 eV are ultimately the most abundant of the secondary species generated by the primary high-energy ionizing radiation [3], the importance of a clear understanding of low-energy electron interactions with biologically relevant molecules is manifest, and may lead to insight into many aspects of the biological effects of radiation [4]. However, obtaining absolute experimental reaction rates for complex bio-molecules is notoriously challenging and hence it is important to benchmark state-of-the-art theory against experimental results, such as elastic scattering, excitation, and ionization, from other relatively simple, model molecules or biological analogues.

Pyrimidine ($C_4H_4N_2$) is a heterocyclic, aromatic organic compound containing two nitrogen atoms at positions 1 and 3 of the six-member ring [5] (see Fig. 1) and is considered as a model molecule for studies of electron interactions with DNA and RNA bases [6] due to the similarity of its ring structure to three of the five nucleobases, namely, cytosine ($C_4H_5N_3O$), thymine ($C_5H_6N_2O_2$), and uracil ($C_4H_4N_2O_2$). As discussed by Zecca *et al.* [7], pyrimidine also possesses some interesting physico-chemical properties that make it an appealing molecule to study from a fundamental perspective. These include a relatively large dipole polarizability and dipole moment [7], and an electron charge cloud with a significant spatial extension.

There have been several studies of electron interactions with pyrimidine in recent years. For example, a study of the electronic states of pyrimidine using vacuum ultraviolet (VUV) absorption, near-threshold electron energy-loss, and *ab initio* multi-reference configuration calculations, was reported by Palmer *et al.* [9]. Levesque *et al.* [6] measured absolute vibrational and electronic-state cross sections for low-energy electron scattering from pyrimidine condensed on a thin film of solid argon at 18 K. The first absolute differential cross section (DCS) measurements for elastic scattering from pyrimidine in the energy range 50-300 eV, were subsequently reported by Maljkovic *et al.* [8]. There was a good level of agreement between the experimental and theoretical results in their study. Cross sections calculated using an independent atom model with a screened additivity rule correction [7] were seen to agree well with the measured values reported in [8] . In addition, we also note that Ferreira da Silva *et al.* [10] reported a study of pyrimidine electronic states by means of VUV absorption and electron

energy-loss spectroscopy and Zecca *et al*. [7] more recently reported experimental total cross sections (TCS) for positron scattering from pyrimidine, accompanied by TCS for the corresponding electron scattering process, again calculated using the independent atom (IAM) approach. To the best of our knowledge, there have been no previous studies of elastic electron scattering from pyrimidine for electron energies below 50 eV.

In the present contribution we report on our absolute experimental elastic DCS results for low-energy electron (3-50 eV) scattering from pyrimidine. Elastic integral cross sections, derived from a molecular phase shift analysis technique [11] are also given. Corresponding cross sections calculated using the *ab initio* Schwinger multichannel variational technique (SMC), and the IAM model are also reported. The Schwinger technique has been successfully applied in recent calculations of elastic scattering, electronic excitation and dissociation in many complex polyatomic molecules of biological relevance, such as 3-hydroxytetrahydrofuran [12], uracil [13], water [14] and pyrazine [15]. The IAM model has been shown to be successful in describing the broad features of elastic scattering cross sections, for a number of complex polyatomic molecules, at energies above about 30 eV [eg. 16,17]. Its particular attraction is that it is a computationally inexpensive approach which provides a good general description of differential elastic scattering and, usually, much better agreement with experiment for the integral cross section at these higher energies.

Details of the experimental apparatus and techniques are explained in the next section, with a description of the theoretical approaches following that. The current results are presented in section 4, with a discussion and detailed comparison with theory and, for a single energy, with previous experimental results [8]. We follow this discussion with some concluding remarks.

2. Experimental apparatus and techniques

A crossed electron-target beam apparatus at the Australian National University has been used to measure elastic electron scattering cross sections from pyrimidine. A detailed description of the experimental setup has been given previously in a number of publications (e.g. [18]), so that only the main points, and more recent system modifications are presented here. Those more recent additions to the spectrometer include a fully computer-controlled hardware system and controlling software to support it [19]. The optimization of the incident electron-beam current and its energy resolution is performed more efficiently with the help of these developments. Additionally, the data acquisition and real time monitoring of all the experimental parameters are handled by the computer-controlled system.

In the present work the spectrometer is operated in two different data collection modes, in order to measure the elastic DCS, and the elastic excitation function (EEF), for electron scattering from pyrimidine. For the DCS measurements, the energy of the incident beam is fixed and the scattered electron analyzer rotated about the molecular beam axis to measure the elastic intensity at fixed angles, within its accessible angular range (see below). For the EEF measurements, the analyzer is fixed at a given angle while the energy of the incident beam is linearly ramped over the energy range of interest and the elastic scattered intensity is simultaneously recorded.

The energy of the incident electron beam is calibrated against the position of the $1s2s^2\ ^2S$ negative ion resonance in elastic electron scattering from He at 19.365 eV [20]. The overall energy resolution of the spectrometer is about 55-65 meV (FWHM), for the present experimental results. Depending on the energy of the electron beam, the incident beam current, as measured with a Faraday cup, varied between 0.5 to 2.0 nA. The electron beam profile and current was optimized under computer control in order to obtain the best possible signal to background ratio for the scattering experiments. The electron spectrometer is capable of measuring DCS and EEF over an angular range of -20º to 130º about the incident electron beam direction. The angular resolution of the present measurements is typically ±1º. The true zero angle position of the analyzer is determined by extrapolating to the maximum of the scattered electron signal from measurements on either side of the mechanical zero position.

A high-purity (99% or better) liquid sample of pyrimidine from Sigma-Aldrich is used to generate the pyrimidine vapor. At room temperature, the vapour pressure above the liquid pyrimidine sample was around 12 Torr, which was sufficient to provide a stable source for the target molecular beam. The pyrimidine sample was also degassed, using several freeze-pump-thaw cycles, under vacuum, before taking the measurements. This was done in order to minimize any possible impurities in the source. The molecular beam is formed by quasi-effusive flow of the gas through a capillary needle, 15 mm long and 0.75 mm in diameter. In the present work, the temperature of the gas lines and valves that controlled the flow of gas, was kept at around 50-60 ºC, while the capillary temperature was elevated to 70 ºC. This helps to prevent condensation of pyrimidine vapor on the inner walls of the gas-lines and valves. The importance of heating the gas handling system, in order to achieve more stable experimental conditions, has been discussed by Maljkovic *et al*. [8], and we concur with their views. Both the pressure and the temperature were monitored and controlled by the new computer-controlled hardware system. The temperature variations during measurements were within ±1 ºC, while the change in the pyrimidine pressure was less than 5%.

The relative flow technique [21] is employed to obtain absolute cross sections by comparing the scattered electron signals from pyrimidine with those from helium. Helium (He) is used as the reference gas as the elastic DCS are now well established, and have been considered as a "benchmark" for many years in this field. For energies below 20 eV, the He cross-sections from the highly accurate variational calculations of Nesbet [22] are used, whereas, for higher energies, the rational function fits of Boesten and Tanaka [23], to a range of previous measurements of the He cross-section, are used. The elastic DCS of pyrimidine (Py) at a given incident electron energy (E_0) and scattered electron angle (θ_0) is derived using the formula;

$$DCS_{Py}\left(E_0,\theta_0\right)=\frac{\left(N_T-N_B\right)F_{He}}{\left(N_{He}-N_B\right)F_{Py}}\sqrt{\frac{M_{He}}{M_{Py}}}\,DCS_{He}\left(E_0,\theta_0\right), \qquad (1)$$

where $DCS_{Py}\ (E_0,\ \theta_0)$ and $DCS_{He}\ (E_0,\ \theta_0)$ are the absolute DCSs for elastic scattering from the target (Py) and reference (He) gases, N_T and N_{He} are the measured scattering signals from the target and He gases (with the background scattering (N_B) contribution being subtracted from both measurements), F_{Py} and F_{He} are the measured relative flow rates and M_{Py} and M_{He} are the molecular weights of Py and He, respectively. Note that all the scattering signals (N_T, N_{He}, N_B) mentioned above are corrected for any variation in the electron beam current during the measurement cycle.

The ratio of the driving pressures between the target and reference gases, is selected to satisfy the condition that the collisional mean free paths are the same for both gases in the beam-forming capillary. This is done to ensure the collision-dependent spatial profile of the gas beams is largely identical in the interaction region. Typical driving pressures of 0.2 Torr for Py and 1.2 Torr for He are used in this experiment to satisfy the pressure ratio condition. The variation in this ratio, caused by any pressure changes during data acquisition, was less than 5% in the present work. The overall uncertainty, both statistical and systematic, of this work is between 7 – 28 %, but for the overwhelming majority of determinations, it lies below 10 %.

3. Theory and computations

3.1 Schwinger multichannel (SMC) calculations

Elastic electron scattering cross sections were computed within the fixed-nuclei approximation using the Schwinger multichannel (SMC) variational procedure [24,25] as implemented for parallel computers [26]. The molecular geometry was first optimized at the level of second-order Möller-Plesset perturbation theory within the 6-31G(*d*) Gaussian basis set using the molecular structure package GAMESS [27], with C_{2v} point-group symmetry assumed. The

unique distances in the optimized geometry are $r(C_2\text{-}N)$=1.3425 Å, $r(C_4\text{-}N)$=1.3441 Å, $r(C_4\text{-}C_5)$=1.3926 Å, $r(C_2\text{-}H)$=1.0878 Å, $r(C_4\text{-}H)$=1.0885 Å, and $r(C_5\text{-}H)$=1.0855 Å, while the unique bond angles are $\angle(HC_2N)$=116.30°, $\angle(HC_4N)$=116.27°, and $\angle(HC_5C_4)$=121.55°. Here the ring atoms are numbered in standard fashion, with the nitrogen atoms at positions 1 and 3.

The SMC calculations were carried out in the single-channel approximation using the 6-311++G(*d,p*) basis set as contained in GAMESS, with the "3*s*" ($x^2+y^2+z^2$) linear combination of Cartesian *d* orbitals excluded. The neutral ground state was computed at the Hartree-Fock level; the computed dipole moment was 2.53 D, compared to a measured value of 2.334 ± 0.010 D [28]. For use in the scattering calculations, the unoccupied orbitals were subjected to an orthogonal transformation to form modified virtual orbitals [29] using a +6 cationic Fock operator. The variational basis set for the scattering calculations included the doublet configuration state functions (CSFs) formed by antisymmetrizing each modified orbital with the closed-shell ground state, as well as those formed by coupling each modified orbital with singlet-coupled single excitations from any of the 15 occupied valence orbitals into any of the 30 lowest-energy modified orbitals. In addition, CSFs of $^2B_1$ symmetry were built by coupling a modified virtual orbital with triplet-coupled single excitations from the 6 highest-energy occupied orbitals into the 30 lowest-energy modified orbitals. The CSFs built on excited states allow for relaxation of the target molecule during the collision (polarization), and the triplet-coupled excitations, in particular, were found to be important in describing the highest-energy π* resonance in the related molecule pyrazine [30, 31]. Separate calculations were carried out for each of the 4 irreducible representations of C_{2v}, and the resulting scattering amplitudes were summed before computing the differential cross sections. Because no correction was made for long-range scattering by the dipole field of pyrimidine, our differential cross sections will not be meaningful at near-forward angles, while the associated integral cross sections should correspond, roughly, to those that would be obtained with the dipole-dominated small-angle scattering omitted.

3.2 Independent atom model calculations

Cross sections for elastic electron scattering from pyrimidine were also calculated using a screening-corrected form of the independent atom model, the IAM model. Each constituent atom of the pyrimidine molecule is represented by a complex potential (i.e. the optical potential), whose real part accounts for the elastic scattering of the incident electrons, while the imaginary part accounts for inelastic collisions with the incident beam. To construct this complex potential for each atom the real part of the potential is represented by the sum of three terms: (i) a static term derived from a Hartree–Fock calculation of the atomic charge distribution [32], (ii) an

exchange term to account for the indistinguishability of the incident and target electrons [33] and (iii) a polarization term [34] for the long-range interactions which depends on the target dipole polarizability (α). The imaginary part, following the procedure of Staszewska *et al* [35], then treats inelastic scattering as electron–electron collisions. Further improvements to the original formulation have been made [36,37] which has led to a model that provides a good approximation for electron–atom scattering over a broad, intermediate energy range.

To calculate the cross sections for electron scattering from pyrimidine, we follow the independent atom method by applying what is commonly known as the additivity rule. In this approach the molecular scattering amplitude is derived from the sum of all the relevant atomic amplitudes, including the phase coefficients, therefore leading to the DCSs for the molecule. Integral cross sections (ICSs) can then be determined by integrating those DCSs, with the sum of the elastic ICS and the absorption ICS (for all inelastic processes except vibrations and rotations) then giving the total cross section (TCS). A limitation of the additivity rule is that the molecular structure is not explicitly considered, so that it is really only applicable when the incident electrons are so fast that they effectively see the target molecule as a sum of the individual atoms (typically above ~100 eV). To reduce this limitation we introduced the screened additivity (SCAR) rule method [38, 39], which considers the geometry of a relevant molecule (atomic positions and bond lengths) by employing some screening coefficients. With this correction the range of validity might be extended to incident electron energies as low as 50 eV. Furthermore, for polar molecules such as pyrimidine, additional dipole-excitation cross sections can be calculated to possibly extend the energy range of validity (~20 eV). This is largely achieved through a better description of the forward angle scattering dominated by the dipole interaction. In the present implementation, rotational excitation cross sections for a free electric dipole are calculated by assuming that the energy transferred is low enough, in comparison to the incident energy, to validate the first Born approximation. Under these circumstances, we have calculated a rotational excitation cross section for $J \rightarrow J'$ for pyrimidine at 300 K by weighting the population for the J^{th} rotational quantum number at that temperature and estimating the average excitation energy from the corresponding rotational constants. The most important effect of this latter correction is a significant increase in the absolute value of the cross section at the lower incident electron energies. Note, finally, that the SCAR+rotation method also includes a procedure where interference terms were normalized (reduced) as much as necessary to ensure that the integrated elastic values also satisfied the (corrected) additivity rule.

4. Results and discussion

Our measured absolute DCS's for elastic scattering of electrons from pyrimidine, are shown in Table 1 along with their associated absolute errors. Also included in Table 1 at the foot of each column are the absolute ICS, for each incident energy, with associated uncertainties. In Fig. 2(a-f), we compare the present DCS measurements at 3, 6, 10, 15, 20 and 50 eV respectively, with cross-sections calculated using the SMC and IAM methods. The only previous DCS measurements we are aware of are those of Maljkovic *et al.* [8] at an energy 50 eV and these are also shown in Fig. 2(f). Our measured and calculated ICS are shown in Fig. 3, while Fig. 4 shows the symmetry components of the SMC calculation. In Fig. 5, we present the current EEF measurements, at scattering angles of 90º and 120º, for the 3 - 15 eV energy range, along with the corresponding DCS measurements.

Our DCS measurements for the lowest energy of 3 eV are shown in Fig. 2(a). The agreement between the measured DCS and the SMC calculation is excellent, with both sets of cross sections at small angles trending to a constant value with decreasing scattering angle. This behavior is also observed in the SMC calculations at 2 eV and 1 eV (not shown here), where the DCS is actually decreasing at the more forward scattering angles at these two energies. This is significantly different behavior from what one might expect due to the large dipole moment and polarizability of the pyrimidine molecule and indicates that other dynamic processes are undoubtedly in play at these low energies (though we still expect the DCS to turn upward at near-zero angles when dipole-scattering effects are considered). At this energy, the results of the IAM model do not agree with the measured DCS or SMC calculation at all and are everywhere larger in magnitude.

At 6 eV (Fig. 2(b)) we again see excellent agreement between the experimental results and the SMC calculation over most of the angular range, with the experimental cross section differing from the theory only at the largest scattering angles (>120°). The IAM model is once again considerably larger than experiment in the mid-angle range but is in good agreement with the data at very forward and backward angles. At both 10 and 15 eV (Figs. 2(c) and 2(d) respectively) we see the angular distribution evolve from one with a single deep minimum at around 90-110° for energies below 6 eV, to a double minimum structure near 60 and 120°, which perhaps indicates dominant d-wave scattering. This angular dependence is also clearly shown in the SMC calculation although, as the energy increases, the absolute magnitude of the calculated cross section becomes a little larger (~30%) than the experimental values at mid to large scattering angles. The shape of the IAM cross section is quite different from both the measured and SMC cross-sections at these energies, although the differences in absolute

magnitude between this calculation and experiment are somewhat smaller than at the lower energies.

At the two highest energies, 20 eV and 50 eV (Figs. 2(e) and 2(f) respectively) the trend observed between experiment and the SMC calculation continues, with the calculation predicting the subtle variations in the angular distribution very well at higher angles, but also predicting a cross section which is at times a factor of two larger than experiment, particularly at 50 eV for angles above about 60°. At both energies, however, the SMC calculation is in excellent agreement with experiment at the more forward scattering angles. In contrast we see the IAM calculation coming into better agreement with experiment at larger angles and, while it does not show the subtle features of the cross section exhibited in the experiment and the SMC calculation, the absolute magnitude is largely in good agreement with experiment at 50 eV. In Fig. 2(f) we also show the only previous experimental result from the Belgrade group [8], and the two experimental cross sections are in excellent agreement, with both results overlapping each other within experimental uncertainties across their common angular range.

It would appear that the main differences between the experimental and SMC results are their magnitudes at intermediate angles and for energies above about 10 eV. Similar differences have also been observed by us in recent measurements of elastic scattering from 3-hydroxy tetrahydrofuran [12]. One reason which has been advanced for this disagreement is that it could be due to the neglect of open inelastic channels in the theory, which could lead to an overestimation of the intermediate energy elastic cross section in the SMC calculation.

As discussed earlier, the IAM method with the screening correction, has been very successful in predicting the elastic DCS for pyrimidine at intermediate and higher energies (see [8]). From Fig. 2 it is evident that the accuracy of this IAM method is greatly reduced as the electron energy decreases, with quite significant differences between it and the experimental results observed at energies below 50 eV. The IAM results we have shown are those for which the dipole correction has been made and, while we do not show the comparison, the model does provide a significantly better description of the scattering than that without the dipole term, particularly for the forward angle cross sections, and even at lower energies.

The elastic integral cross-sections (ICS), given in Table 1, were derived from the present DCS measurements using a molecular phase-shift analysis technique [11], which removes some of the subjectivity from the extrapolation process to those forward and backward angles not covered in the DCS measurements. From Fig. 3 it can be seen that the measured and both calculated ICS's,

are largely in agreement for energies of 10 eV and above, within the uncertainty of the measurements (~ 25%). This is surprising given the differences in the calculated DCS shown in Fig. 2, particularly at larger scattering angles, and is no doubt due, in most part, to the weighting placed on forward scattering in the determination of the ICS. At lower energies the SMC calculation is clearly in better agreement with experiment. The measured and SMC ICS's both peak at around 10 eV.

The strong peak at 4.6 eV in the SMC ICS of Fig. 3 is due to a π^* shape resonance occurring in $^2B_1$ symmetry. Although not easily seen in Fig. 3, there are also two further π^* resonance peaks in the SMC ICS, at 0.38 eV ($^2B_1$ symmetry) and 0.63 eV ($^2A_2$ symmetry). These three resonances are more clearly seen in Fig. 4, where the symmetry components of the SMC ICS are plotted separately and on a logarithmic scale. In an electron transmission measurement, Nenner and Schulz [40] observed the first resonance as a series of vibrational peaks, the first of which falls at 0.25 eV; however, they interpret this peak as an excited vibrational level, with the vibrational ground state being at negative energy (i.e., a bound anion). The onset of the second resonance in the transmission spectrum is at 0.77 eV, and that of the third resonance at 4.24 eV. The SMC resonance energies are in reasonably good agreement with these measured values. We note that, as in the closely-related molecule pyrazine [30,31], the third resonance, though nominally an elastic-channel π^* shape resonance, is in fact likely of mixed character, with significant contributions from core-excited configurations built on low-lying triplet states. We also note that the further peaks seen above 4.6 eV in the SMC cross section are likely all pseudo-resonances, which are typical in such calculations at energies where excitation channels treated as closed are actually open.

The energy dependence of the measured differential cross section at fixed scattering angles of 90° and 120° is shown over the 3–15 eV energy range in Fig. 5, along with points taken from the angular scans at each of the four energies in this range. The agreement between the results obtained in these two modes of operation of the spectrometer, which were discussed above, is excellent, indicating a good level of self-consistency within our measurements. The EEF at 90° suggests a peak at around 4.2 eV, while the corresponding peak in the 120° EEF is possibly located at around 4.5 eV. These energies are consistent with the location of the third π^* resonance in the transmission measurements of Nenner and Schulz [40] and in the ICS computed by the SMC method, discussed in the preceding paragraph. Both EEFs also exhibit broad maxima between roughly 6 and 11 eV, and there appear to be two narrower, weak features at 10 and 12 eV in the 90° EEF curve.

5. Conclusion

The present study provides the first experimental and theoretical data for low-energy (< 50 eV) elastic scattering of electrons from the pyrimidine molecule, a model molecule for the nucleo-bases thymine, cytosine, and uracil. These results should be significant, for example, in modeling studies of charged-particle tracks in biological media, where absolute elastic cross sections, together with energy loss spectra, can be used to determine inelastic scattering cross sections which are critical inputs to Monte-Carlo modeling codes.

The experimental results and Schwinger variational calculations are in very good agreement at both the DCS and ICS level of comparison, particularly at the lower energies in the case of the DCS. The comparison with experiment of the present IAM calculations reveal the limitations of this approach, at energies below 50 eV, in predicting differential scattering cross sections. While we do not show the details, the addition of the dipole correction to this model markedly improves the level of agreement with experiment at forward angles and also results in better predictive capacity of this method at the ICS level, even down to relatively low energies (10 eV). This is a consequence of the fact that the majority of the contribution to the elastic ICS arises from the forward angle part of the elastic DCS. We also note that the π^* resonance at around 4.5 eV, that is predicted by the Schwinger variational calculations, has been seen in an electron transmission study [40].

Acknowledgements

The Support of the Australian Research Council, The International Science Linkage program of the Australian Government, the Spanish Ministerio de Ciencia e Innovación (Project FIS2009-10245), and the EU Framework Programme (COST Action MP1002) is gratefully acknowledged. The work of VM and CW was supported by the Chemical Sciences, Geosciences, and Biosciences Division, Office of Basic Energy Sciences, Office of Science, US Department of Energy under Grant No. DE-FG02-97ER14814, and employed the Supercomputing and Visualization Facility at the Jet Propulsion Laboratory.

References

[1] M. Fuss and G. Garcia, *Radiation Damage in Biomolecular Systems* (Berlin: Springer, 2011).

[2] B. Boudaiffa, P. Cloutier, D. Hunting, M.A. Huels, and L. Sanche, *Science* **287**, 1658 (2000).

[3] F. Martin, P. D. Burrow, Z. Cai, P. Cloutier, D. Hunting, and L. Sanche, *Phys. Rev. Lett.* **93**, 068101 (2004).

[4] B. D. Michael and P. O. Neil, *Science* **287**, 1603 (2000).

[5] T. L. Gilchrist, *Heterocyclic Chemistry*, 3rd ed. (Prentice Hall, New Jersey, 1997).

[6] P. L. Levesque, M. Michaud, and L. Sanche, *J. Chem. Phys*. **122**, 094701 (2005).

[7] A. Zecca, L. Chiari, G. García, F. Blanco, E. Trainotti, M. J. Brunger, *J. Phys. B* **43**, 215204 (2010).

[8] J. B. Maljkovic, A. R. Milosavljevic, F. Blanco, D. Sevic, G. Garcia, and B. P. Marinkovic, *Phys. Rev. A* **79**, 052706 (2009).

[9] M. H. Palmer, I. C. Walker, M. F. Guest, and A. Hopkirk, *Chem. Phys.* **147**, 19 (1990).

[10] F. Ferreira da Silva, D. Almeida, G. Martins, A. R. Milosavljevic, B. P. Marinkovic, S. V. Hoffmann, N. J. Mason, Y. Nunes, G. Garcia, and P. Limao-Vieira, *Phys. Chem. Chem. Phys.* **12**, 6717 (2010).

[11] L Campbell, M J Brunger, A M Nolan, L J Kelly, A B Wedding, J Harrison, P J O Teubner, D C Cartwright, and B McLaughlin, *J. Phys. B* **34**, 1185 (2001).

[12] V. Vizcaino, J. Roberts, J.P. Sullivan, M.J. Brunger, S.J. Buckman, C. Winstead, and V. McKoy New Journal of Phys. **10**, 053002 (2008)

[13] C. Winstead and V. McKoy J. Chem. Phys. **128**, 174302 (2008)

[14] M.A. Khakoo, H. Silva, J. Muse, M.C.A. Lopes, C. Winstead, and V. McKoy Phys. Rev. A **78**, 052710 (2008)

[15] C. Winstead and V. McKoy Phys. Rev. Letts. **98**, 113201 (2007)

[16] H. Kato, T. Asahina, H. Masui, M. Hoshino, H. Tanaka, H. Cho, O. Ingolfsson, F. Blanco, G. Garcia, S.J. Buckman, and M.J. Brunger J. Chem. Phys. **132** 074309 (2010)

[17] L.R. Hargreaves, J.R. Brunton, A. Prajapati, M. Hoshino, F. Blanco, G. Garcia, S.J Buckman and M.J. Brunger J. Phys.B: At. Mol. Opt. Phys. **44** 045207 (2011)

[18] J. C. Gibson, L. A. Morgan, R. J. Gulley, M. J. Brunger, C. T. Bundschu, and S. J. Buckman, *J. Phys. B* **29**, 3197 (1996).

[19] V. Vizcaino, Ph.D. thesis (Australian National University, unpublished, 2008).

[20] A. Gopalan, J. Bommels, S. Gotte, A. Landwehr, K. Franz, M.-W. Ruf, H. Hotop, and K. Bartschat, *Eur. Phys. J. D* **22**, 17 (2003).

[21] M. J. Brunger and S. J. Buckman, *Phys. Rep.* **357**, 215 (2002).

[22] R. K. Nesbet, *Phys. Rev. A* **20**, 58 (1979).

[23] L. Boesten and H. Tanaka, *At. Data Nucl. Data Tables* **52**, 25, (1992).

[24] K. Takatsuka and V. McKoy, *Phys. Rev. A* **24**, 2473 (1981).

[25] K. Takatsuka and V. McKoy, *Phys. Rev. A* **30**, 1734 (1984).

[26] C. Winstead and V. McKoy, *Adv. At., Mol., Opt. Phys.* **36**, 183 (1996).

[27] M. W. Schmidt, K. K. Baldridge, J. A. Boatz, S. T. Elbert, M. S. Gordon, J. H. Jensen, S. Koseki, N. Matsunaga, K. A. Nguyen, S. J. Su, T. L. Windus, M. Dupuis, and J. A. Montgomery, *J. Comput. Chem.* **14**, 1347 (1993).

[28] G. L. Blackman, R. D. Brown, and F. R. Burden, *J. Mol. Spectrosc.* **35**, 444 (1970).

[29] C. W. Bauschlicher, *J. Chem. Phys*. **72**, 880 (1980).

[30] C. Winstead, and V. McKoy, *Phys. Rev. Lett.* **98**, 113201 (2007).

[31] C. Winstead, and V. McKoy, *Phys. Rev. A* **76**, 012712 (2008).

[32] R.D. Cowan, *The Theory of Atomic Structure and Spectra* (London: University of California Press, 1981)

[33] M. E. Riley and D. G. Truhlar, *J. Chem. Phys*. **63**, 2182 (1975).

[34] X. Z. Zhang, J. F. Sun, and Y. F. Liu, *J. Phys. B: At. Mol. Opt. Phys.* **25** 1893 (1992)

[35] G. Staszewska, D. W. Schwenke, D. Thirumalai, and D. G. Truhlar, *Phys. Rev.* A **28** 2740 (1983).

[36] F. Blanco and G. Garcia, *Phys. Lett.* A **295,** 178 (2002).

[37] F. Blanco and G. Garcia, *Phys. Rev.* A **67,** 022701 (2003).

[38] F. Blanco and G. Garcia, *Phys. Lett.* A **330,** 230 (2004).

[39] F. Blanco and G. Garcia, *J. Phys. B: At. Mol. Opt. Phys.* **42,** 145203 (2009).

[40] I. Nenner and G. J. Schulz, J. Chem. Phys **62**, 1747 (1975)

TABLE 1. Absolute experimental DCS for elastic scattering from pyrimidine in units of 10^{-16} cm^2 sr^{-1}. The uncertainty is given in parentheses (%). The ICS for each incident energy is given in units of 10^{-16} cm^2 at the base of each column. The uncertainty of ICS is estimated to be around 25%.

Scattering angle (deg)	Incident Energy (eV)						
	3	6	10	15	20	30	50
10							45.5 (9.6)
15						27.5 (7.5)	
20		10.0 (28)	29.1 (18)	18.1 (13)	17.0 (8.1)	12.9 (7.4)	6.73 (7.5)
25			20.1 (15)				
30		7.51 (14)	8.55 (9.4)	7.95 (7.4)	5.94 (7.7)	2.51 (7.4)	1.42 (7.7)
40	4.42 (25)	6.26 (7.7)	4.40 (7.3)	2.50 (7.4)	1.52 (7.7)	1.06 (7.5)	1.04 (7.8)
50	4.35 (14)	4.49 (7.5)	2.59 (7.2)	1.12 (7.3)	0.720 (7.8)	0.824 (8.0)	0.761 (7.7)
60	3.99 (7.4)	3.25 (7.3)	1.73 (7.3)	0.983 (7.2)	0.704 (7.4)	0.743 (7.3)	0.383 (7.3)
70	3.35 (7.5)	2.12 (7.6)	1.44 (7.2)	1.06 (7.2)	0.815 (7.4)	0.582 (7.6)	0.255 (7.7)
80	2.75 (7.4)	1.47 (7.4)	1.44 (7.2)	1.15 (7.2)	0.786 (7.3)	0.471 (7.3)	0.268 (7.7)
90	1.70 (8.3)	1.28 (7.6)	1.51 (7.2)	1.12 (7.2)	0.666 (7.3)	0.451 (7.4)	0.252 (8.3)
100	1.38 (7.5)	1.34 (7.5)	1.70 (7.2)	1.02 (7.3)	0.672 (7.2)	0.512 (7.4)	0.266 (7.5)
110	1.19 (7.4)	1.54 (7.5)	1.81 (7.2)	0.920 (7.2)	0.703 (7.3)	0.663 (12)	0.316 (7.9)
120	1.24 (7.7)	1.82 (7.4)	1.68 (7.3)	0.952 (7.2)	0.784 (7.5)	1.93 (9.0)	0.405 (7.5)
129	1.64 (12)	2.00 (7.6)	1.64 (7.2)	1.15 (7.2)	1.04 (7.3)	2.93 (8.7)	0.491 (7.5)
ICS	37.5	35.0	45.0	37.1	35.9	30.7	16.7

Figure Captions

Figure 1. (Color online) Schematic diagram showing the structure of the pyrimidine molecule and pyrimidine nucleobases [8].

Figure 2. (Color online) Absolute DCS (10^{-16} cm^2 sr^{-1}) for elastic electron scattering from pyrimidine at (a) 3 eV, (b) 6 eV, (c) 10 eV, (d) 15 eV, (e) 20 eV, and (f) 50 eV. The present measurements are shown as full circles, while previous measurements [8] are shown as triangles in (f). The present theoretical DCS calculated using the SMC method are shown as a solid curve, and the IAM-SCAR calculations are shown as a dashed curve.

Figure 3. (Color online) Present experimental and theoretical ICS (10^{-16} cm^2). The experimental cross sections are shown as full circles, the SMC results as a solid curve, and the IAM-SCAR results as a dashed curve.

Figure 4. (Color online) Symmetry components of the integral elastic cross section for electron scattering by pyrimidine as obtained from the present SMC calculations. The curves are labeled according to the representations of the C_{2v} point group, and the peaks corresponding to three π^* resonances are also indicated.

Figure 5. (Color online) Absolute DCS (10^{-16} cm^2 sr^{-1}) shown as a function of energy (EEF) for the energy range of 3-15 eV at scattering angles of (a) 90° and (b) 120°. Also shown are the angular DCS measurements taken at discrete energies in the range of interest.

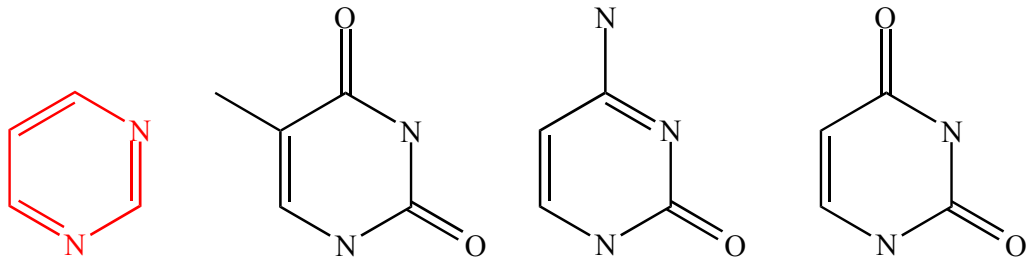

Pyrimidine Thymine Cytosine Uracil

Figure 1

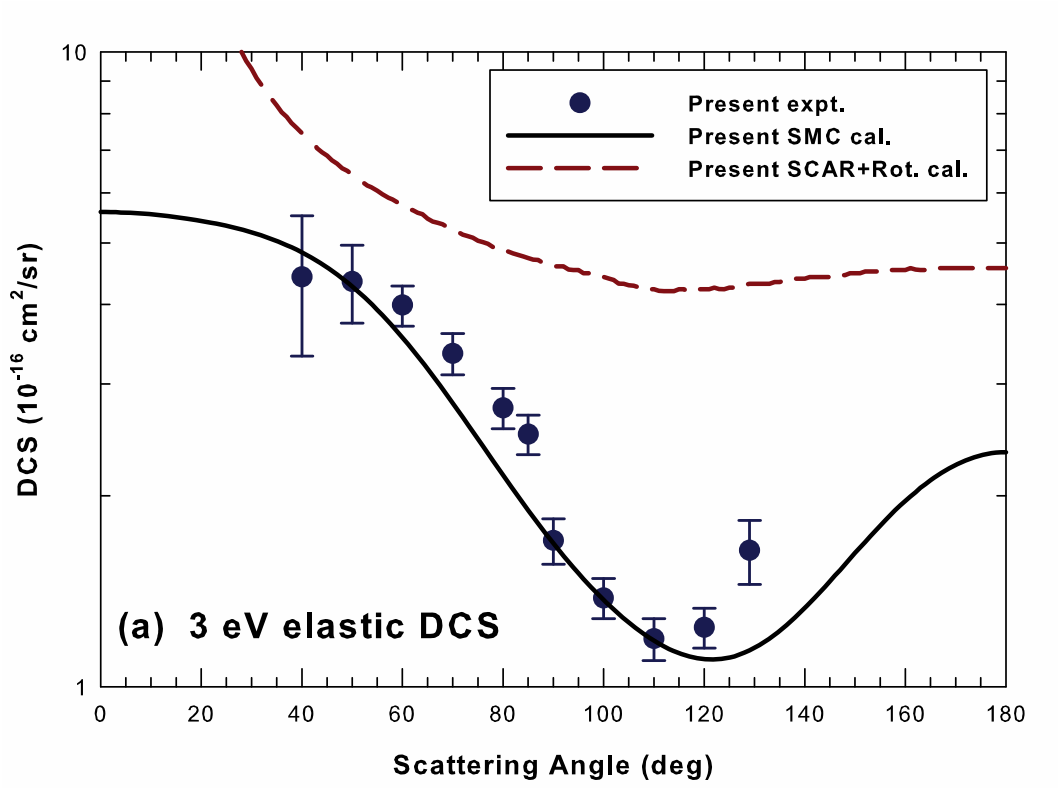
Present expt.
Present SMC cal.
Present SCAR+Rot. cal.
(a) 3 eV elastic DCS
DCS (10^-16 cm^2/sr)
Scattering Angle (deg)
10
1
0
20
40
60
80
100
120
140
160
180

Figure 2(a)

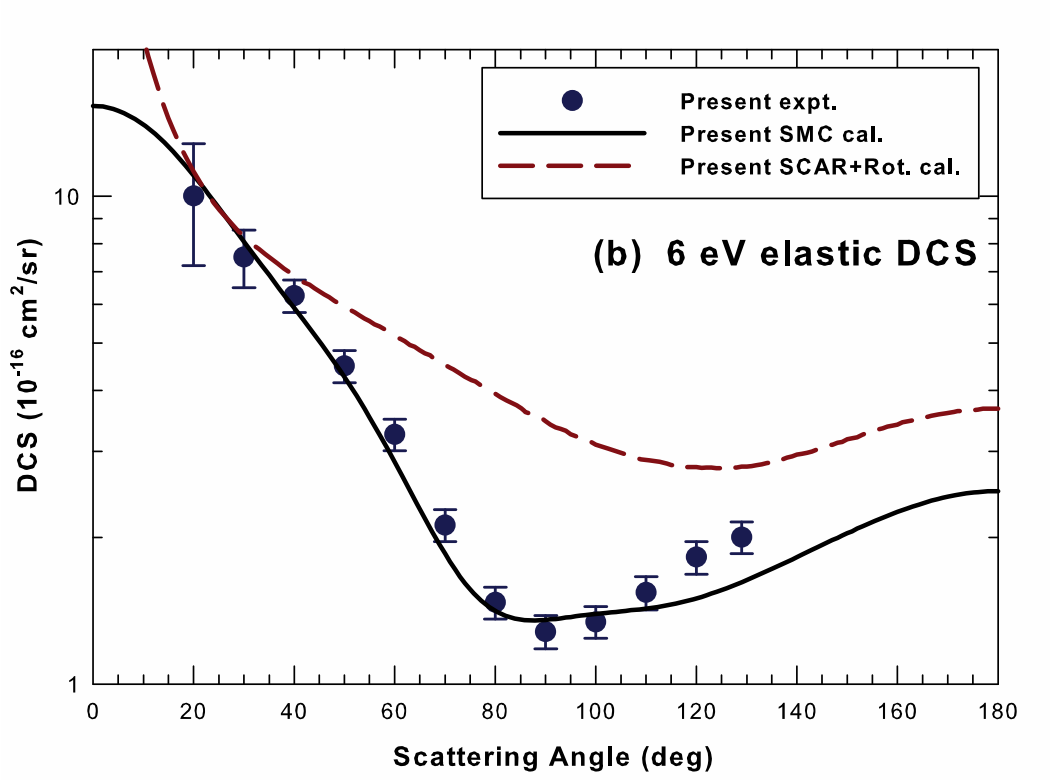
Present expt.
Present SMC cal.
Present SCAR+Rot. cal.
(b) 6 eV elastic DCS
DCS (10^{-16} cm^2/sr)
Scattering Angle (deg)
10
1
0
20
40
60
80
100
120
140
160
180

Figure 2(b)

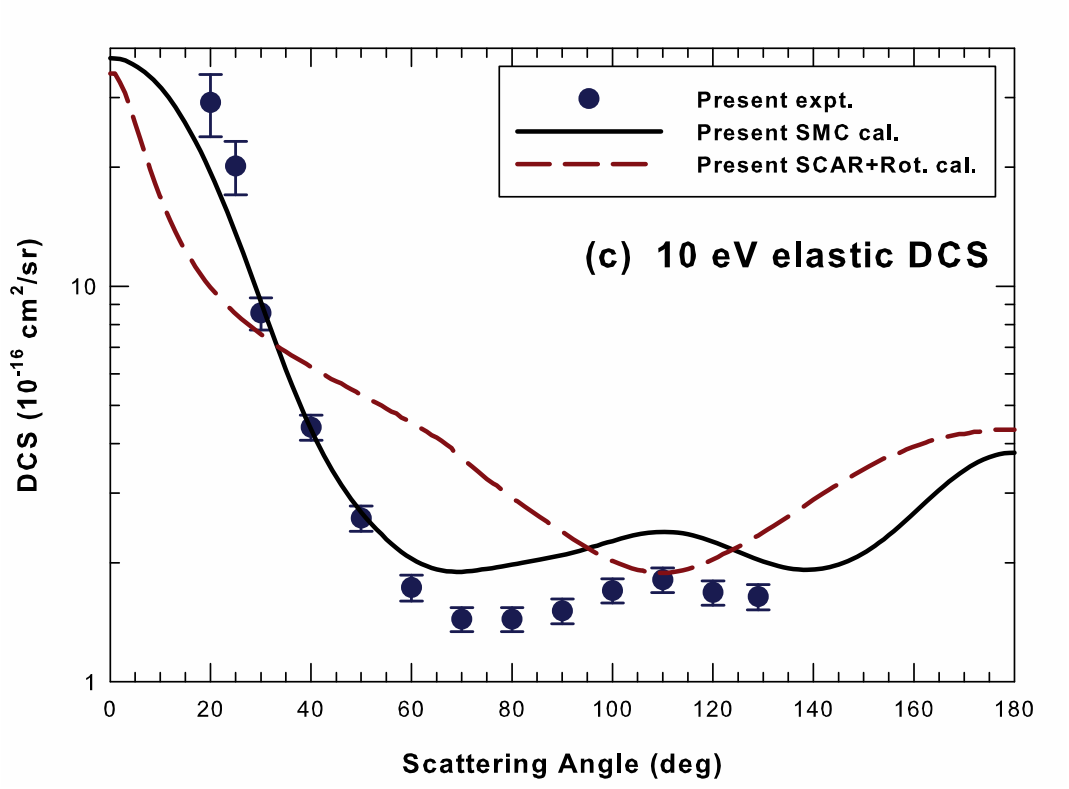
Present expt.
Present SMC cal.
Present SCAR+Rot. cal.
(c) 10 eV elastic DCS
DCS (10^-16 cm^2/sr)
10
1
0
20
40
60
80
100
120
140
160
180
Scattering Angle (deg)

Figure 2(c)

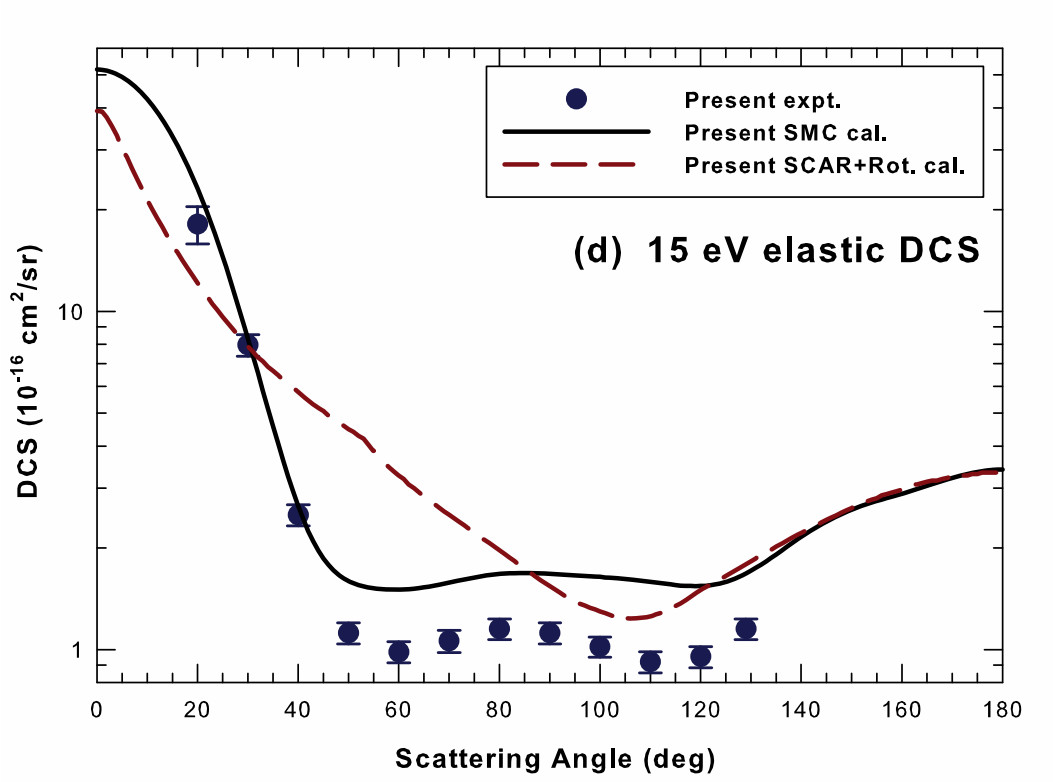
Present expt.
Present SMC cal.
Present SCAR+Rot. cal.
(d) 15 eV elastic DCS
DCS (10^{-16} cm^2/sr)
10
1
0
20
40
60
80
100
120
140
160
180
Scattering Angle (deg)

Figure 2(d)

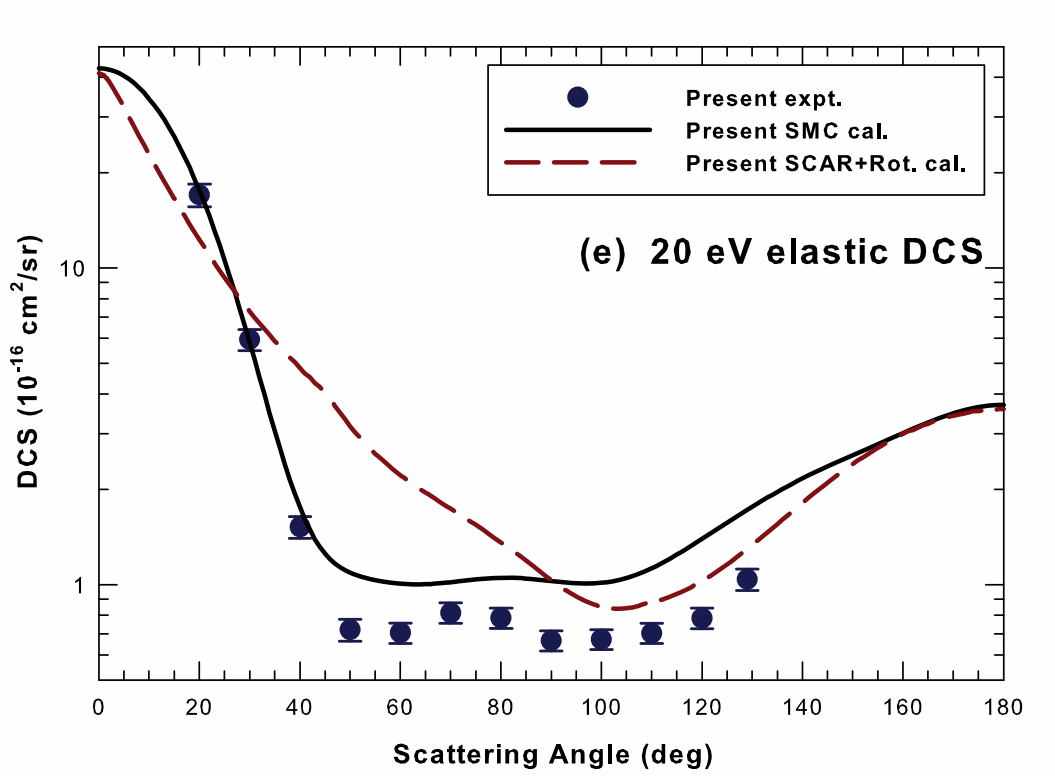
Present expt.
Present SMC cal.
Present SCAR+Rot. cal.
(e) 20 eV elastic DCS
DCS (10^{-16} cm^2/sr)
10
1
0
20
40
60
80
100
120
140
160
180
Scattering Angle (deg)

Figure 2(e)

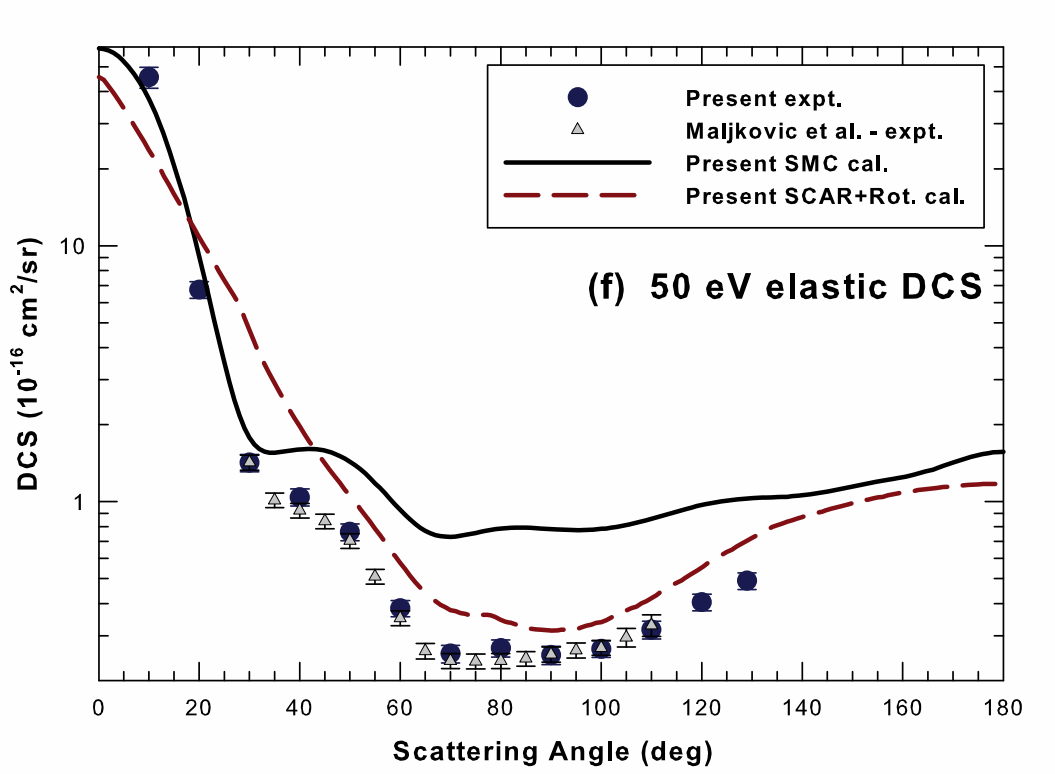
Present expt.
Maljkovic et al. - expt.
Present SMC cal.
Present SCAR+Rot. cal.
(f) 50 eV elastic DCS
DCS (10^{-16} cm^2/sr)
10
1
0
20
40
60
80
100
120
140
160
180
Scattering Angle (deg)

Figure 2(f)

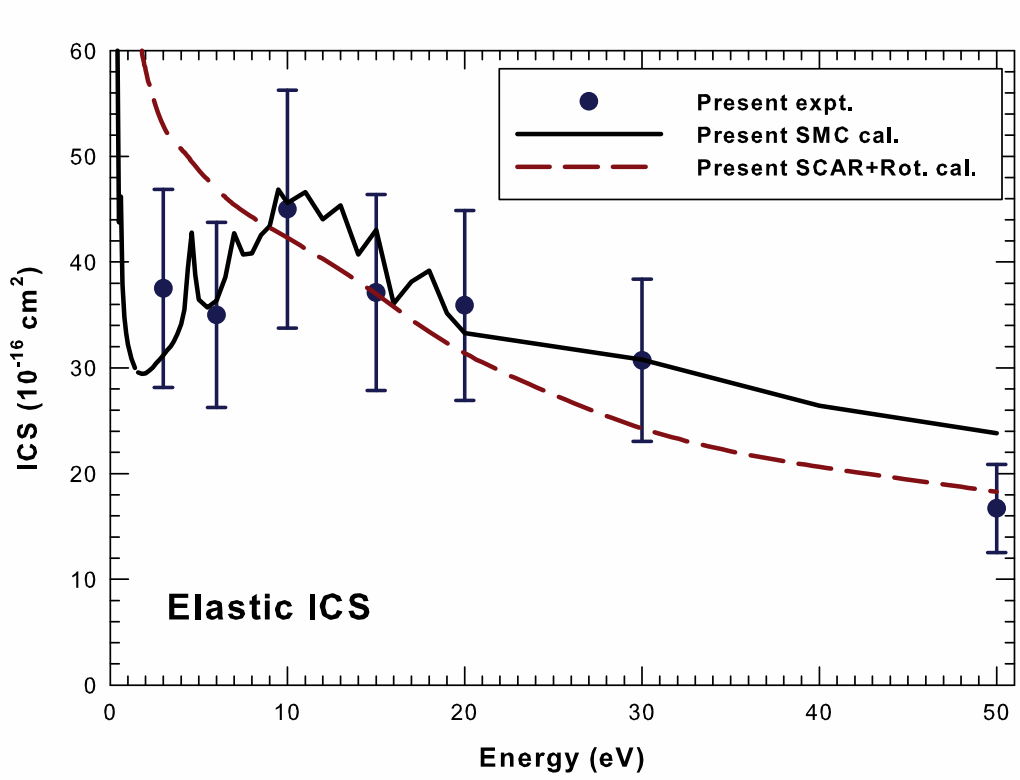
Present expt.
Present SMC cal.
Present SCAR+Rot. cal.
Elastic ICS
ICS (10^{-16} cm^2)
Energy (eV)
0
10
20
30
40
50
60

Figure 3

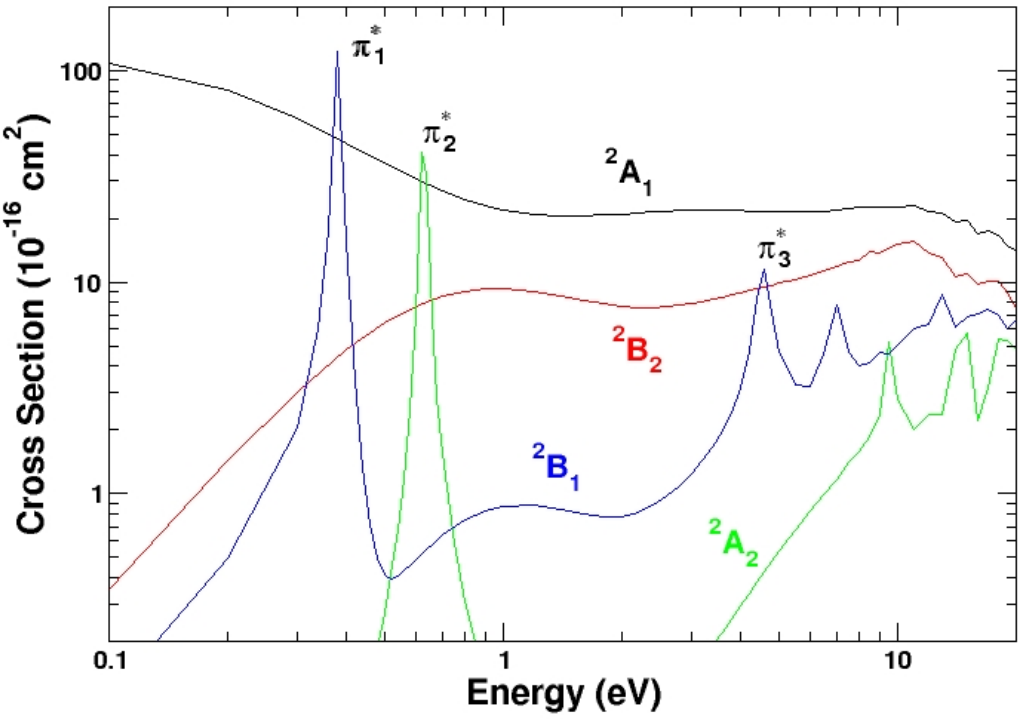
Cross Section (10^{-16} cm^2)
100
10
1
0.1
1
10
Energy (eV)
π^*_1
π^*_2
π^*_3
$^2A_1$
$^2B_2$
$^2B_1$
$^2A_2$

Figure 4

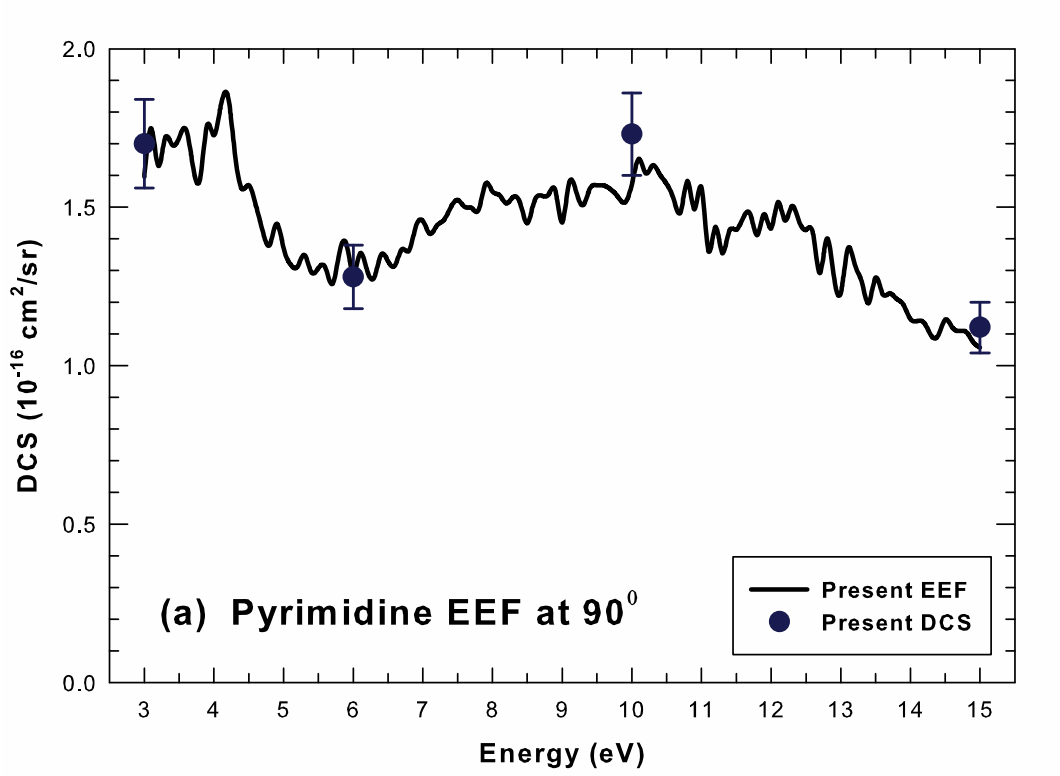

Figure 5(a)

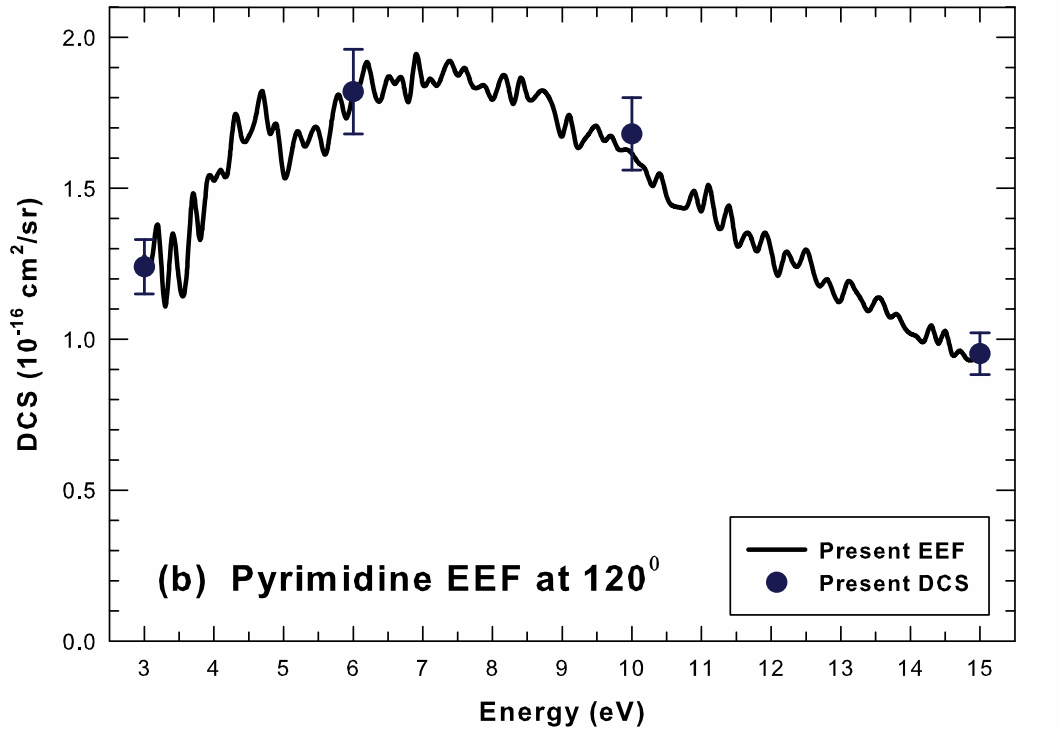

Figure 5(b)